



HAL
open science

Using data and models to infer climate and environmental changes during the Little Ice Age in tropical West Africa

Anne-Marie Lézine, Maé Catrain, Julian Villamayor, Myriam Khodri

► **To cite this version:**

Anne-Marie Lézine, Maé Catrain, Julian Villamayor, Myriam Khodri. Using data and models to infer climate and environmental changes during the Little Ice Age in tropical West Africa. *Climate of the Past*, 2023, 19 (1), pp.277-292. 10.5194/cp-19-277-2023 . hal-03968203

HAL Id: hal-03968203

<https://hal.science/hal-03968203v1>

Submitted on 3 Feb 2023

HAL is a multi-disciplinary open access archive for the deposit and dissemination of scientific research documents, whether they are published or not. The documents may come from teaching and research institutions in France or abroad, or from public or private research centers.

L'archive ouverte pluridisciplinaire **HAL**, est destinée au dépôt et à la diffusion de documents scientifiques de niveau recherche, publiés ou non, émanant des établissements d'enseignement et de recherche français ou étrangers, des laboratoires publics ou privés.



Distributed under a Creative Commons Attribution 4.0 International License



Using data and models to infer climate and environmental changes during the Little Ice Age in tropical West Africa

Anne-Marie Lézine¹, Maé Catrain¹, Julián Villamayor^{1,2}, and Myriam Khodri¹

¹Laboratoire d'Océanographie et du Climat, Expérimentation et Approche numérique/IPSL, Sorbonne Université – CNRS-IRD-MNHN, 4 Place Jussieu, 75005 Paris, France

²Department of Atmospheric Chemistry and Climate, Institute of Physical Chemistry Rocasolano, CSIC, Madrid, Spain

Correspondence: Anne-Marie Lézine (anne-marie.lezine@locean.ipsl.fr)

Received: 22 July 2022 – Discussion started: 18 August 2022

Revised: 19 December 2022 – Accepted: 23 December 2022 – Published: 1 February 2023

Abstract. Here we present hydrological and vegetation paleo-data extracted from 28 sites in West Africa from 5° S to 19° N and the past1000/PMIP4 IPSL-CM6A-LR climate model simulations covering the 850–1850 CE period to document the environmental and climatic changes that occurred during the Little Ice Age (LIA). The comparison between paleo-data and model simulations shows a clear contrast between the area spanning the Sahel and the savannah in the north, characterized by widespread drought, and the equatorial sites in the south, where humid conditions prevailed. Particular attention was paid to the Sahel, whose climatic evolution was characterized by a progressive drying trend between 1250 and 1850 CE. Three major features are highlighted: (1) the detection of two early warning signals around 1170 and 1240 CE preceding the onset of the LIA drying trend; (2) a tipping point at 1800–1850 CE characterized by a rainfall drop and an environmental degradation in the Sahel; and (3) a succession of drying events punctuating the LIA, the major one of which was dated to around 1600 CE. The climatic long-term evolution of the Sahel is associated with a gradual southward displacement of the Inter-Tropical Convergence Zone induced by the radiative cooling impacts of major volcanic eruptions that have punctuated the last millennium.

1 Introduction

Precipitation in tropical West Africa is closely related to the West African Monsoon (WAM) system, created by the temperature land–sea contrast between the tropical Atlantic and the west of the African continent (Nicholson, 2013) and is

also influenced by the migration of the Inter-Tropical Convergence Zone (ITCZ, Gadgil 2018). The WAM long-term variability during the 20th century has focused much attention due to the severe consequences in the Sahel semi-arid region, which experienced a long period of drought in the 1970s–1980s (Folland et al., 1986; Giannini et al., 2003). It is broadly accepted that these changes were mainly driven by the sea surface temperature (SST) variability (Folland et al., 1986; Mohino et al., 2011; Rodríguez-Fonseca et al., 2015), amplified by land surface processes (Giannini et al., 2003; Kucharski et al., 2013). However, only a few works document the WAM variability prior to the 20th century (Nicholson et al., 2012; Gallego et al., 2015; Villamayor et al., 2018) due to the little information covering the 19th century and beyond. The paleo-archives are rare and often incomplete and suffer from often poorly constrained chronologies. Moreover, these archives are rarely direct records of climate parameters but indirect ones, namely historical, biological or sedimentological. They integrate not only changes in environmental parameters but also the vital effect of species, the vulnerability or the resilience of ecosystems and the cultural adaptations of populations. Here we use pollen and other environmental proxies as well as historical chronicles to document the last millennium with a special focus on the period from 1250 to 1850 CE including the transition between the Medieval Climate Anomaly (MCA; 950–1250 CE) and the Little Ice Age (LIA; 1450–1850 CE) periods characterized by global temperatures, respectively, above and below average (Nash et al., 2016). The aim of this research is not to record the climate variability at an interannual scale but to discuss the timing, distribution and magnitude of the major

secular environmental changes which punctuated the LIA in northern tropical Africa with a focus on the regional biomes and hydrological systems responses times to rainfall anomalies.

2 Material and method

2.1 Paleo-data

This paper uses compilations of paleo-records from different sources with the highest available resolution (Table 1; Fig. 1). These data have the advantage of providing continuous records over the last millennium, but their temporal resolution is generally mostly (multi)decadal to centennial: pollen data are used for vegetation reconstructions (Elenga, 1992; Reynaud-Farrera et al., 1996; Ballouche, 1998; Vincens et al., 1998; Salzmann and Hoelzmann, 2005; Ngomanda et al., 2007; Waller et al., 2007; Brncic et al., 2009, 2007; Lézine et al., 2011, 2013, 2019; Lebamba et al., 2016; Tovar et al., 2019; Fofana et al., 2020; Catrain, 2021) and micropaleontological, sedimentological and geochemical data to capture hydrological and climatic changes (Bertaux et al., 1998; Holmes et al., 1999; Street-Perrott et al., 2000; Schefuß et al., 2005; Wang et al., 2008; Shanahan et al., 2009; Mulitza et al., 2010; Nguetsop et al., 2010, 2011, 2013; Carré et al., 2019; Lézine et al., 2019; Fofana et al., 2020; Catrain, 2021). Compilations of historical chronicles (Nicholson, 1978, 1980, 2013; Nicholson et al., 2012; Coquery-Vidrovitch, 1997; Maley and Vernet, 2013) and instrumental records (Gallego et al., 2015) have also been examined, although the first are based on records of extreme events only (droughts, floods) and the second are limited in their temporal coverage. All these data are also scattered in a few limited areas of the Sahel (Senegal, southern Mauritania, Niger River inner loop, Lake Chad basin) with possible redundancies.

The resulting data set is highly heterogeneous. Therefore, the data have been homogenized as follows: (1) only records covering the interval between 900 CE and the present day with at least a 100-year temporal resolution have been taken into account; (2) in order to evaluate the relative amplitude of the environmental and climate change, we build a six-point scale ranging from 0, corresponding to the most arid environment (e.g., drying of lakes, salinization of water, increase in dust transport, bare soils) or the driest climate, up to 6, which refers to the most humid environment (e.g., high lake level, fresh water, dense forest) or the wettest climate. Decimal values were selectively added to identify minor changes in the paleoenvironment. This approach, based on our own expertise, provides a *qualitative* description of regional environmental and climatic conditions. It emphasizes the major stages of environmental change while eliminating minor noisy variations (see Fig. S1 in the Supplement).

In order to verify whether the methodology employed provides reliable indications of environmental change for the pe-

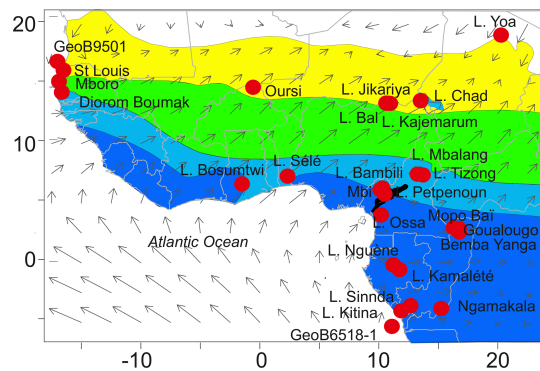


Figure 1. Map showing the location of paleo-records available in tropical West Africa documenting the last millennium (Table 1). Gray arrows indicate the strength and direction of the main 925 hPa monsoonal winds during boreal summer, i.e., the WAM rainy season (NCEP-DOE AMIP-II Reanalysis; Kanamitsu et al., 2002). In color, vegetation units from White (1983): dark blue, Guineo-Congolian rainforest; light blue, Sudano-Guinean woodland and wooded grassland (here referred to as savannah (vegetation) zone); green, Sudanese woodland and wooded grassland; yellow, Sahelian grassland and wooded grassland; black, Afromontane forest.

riod prior to the instrumental records, scores of the WAM rainy season (July to September), multidecadal hydrological changes from natural archives and historical data (Table 1) in the Sahel are compared to the African Southwesterly Index (ASWI) developed by Gallego et al. (2015) over 1840–1990 CE. The ASWI is based on JAS (January, August, September) wind direction data (i.e., the persistence of the low-level southwesterly winds) from historical measurements available since 1839 in a region over the Atlantic, close to West Africa (7–13° N, 29–17° W). The ASWI is strongly correlated with the observed Sahel precipitation since 1900 and is, therefore, presented as a good indicator of its variability. It was validated against instrumental observations as a good measure of WAM intensity during the rainy season over the instrumental period (Gallego et al., 2015). Positive values of the ASWI indicate periods when the monsoon is well established over the Sahel, and thus they define periods of heavy rainfall in the region, which is consistent with observational data (Descroix et al., 2015). As previously shown by Villamayor et al. (2018), there are strong similarities between the historical rainfall records in the Sahel and ASWI. However, Fig. 2 shows that historical records (yellow curve, Fig. 2a) give a slightly different magnitude of dry and wet anomalies that reflects the sensitivity of populations to periods of drought or flooding. Our assessment of hydrological conditions based on natural archives (blue curve, Fig. 2a) reflects historical record variations but with a somewhat weaker magnitude. This is probably due to the much lower temporal resolution of the available data (25–50 years on average). It is also worth noting that the lake data correspond to a precipitation and evaporation balance and not the

Table 1. Geographical positions, type and references of paleo-records used in this study (see Fig. 1).

Site name	Proxy	Latitude	Longitude	Reference	Sector/ vegetation zones
Lake Yoa	Pollen/sediment	19.057621	20.500690	Lézine et al. (2011)	Sahara (desert)
GeoB9501	Dust fraction	16.83333	−16.73333	Mulitza et al. (2010)	Sahel
St Louis	Pollen/diatom	16.03508	−16.48382	Fofana et al. (2020)	Sahel (grasslands and wooded grasslands)
Mboro (Baobab)	Pollen/diatom	15.149132	−16.909275	Lézine et al. (2019)	Sahel (grasslands and wooded grasslands)
Oursi	Pollen	14.65283	−0.486	Ballouche (1998)	Sahel (grasslands and wooded grasslands)
Diorom Boumak	Geochemistry	13.835809	−16.498372	Carré et al. (2019)	Sahel/savannah boundary
Lake Jikariya	Sediment/mineral–magnetic	13.3136667	11.077	Waller et al. (2007), Wang et al. (2008)	Sahel (grasslands and wooded grasslands)
Lake Bal	Ostracods/chemistry	13.304	10.943	Holmes et al. (1999)	Sahel (grasslands and wooded grasslands)
Lake Kajemarum	Dust fraction/Geochemistry	13.303	11.024	Street-Perrott et al. (2000)	Sahel (grasslands and wooded grasslands)
Lake Chad	Historical	13.053472	14.463469	Maley and Vernet (2013)	Sahel (grasslands and wooded grasslands)
Lake Mbalang	Pollen/diatoms	7.316	13.733	Vincens et al. (2010), Nguetsop et al. (2011)	Savannah
Lake Tizong	Pollen/diatoms	7.25	13.583	Nguetsop et al. (2013), Lebamba et al. (2016)	Savannah
Lake Sélé	Pollen	7.15	2.433	Salzmann and Hoelzmann (2005)	Savannah
Lake Bosumtwi	Geochemistry	6.5	−1.416	Shanahan et al. (2009)	Central Africa (lowlands) (equatorial forests)
Mbi	Pollen	6.089273	10.348549	Lézine et al. (2020)	Central Africa (highlands) (Afromontane forests)

Table 1. Continued.

Site name	Proxy	Latitude	Longitude	Reference	Sector/ vegetation zones
Lake Bambili	Pollen/geochemistry	5.936	10.242	Lézine et al. (2013)	Central Africa (highlands) (Afromontane forests)
Lake Petpenoun	Pollen	5.64147	10.64531	Catrain (2021)	Savannah
Lake Ossa	Pollen/diatoms	3.800	10.75	Reynaud-Farrera et al. (1996), Nguetsop et al. (2010)	Central Africa (lowlands) (equatorial forests)
Mopo Bai	Pollen/geochemistry	2.240	16.261388	Brncic et al. (2009)	Central Africa (lowlands) (equatorial forests)
Bemba Yanga	Pollen	2.18726	16.52513	Tovar et al. (2019)	Central Africa (lowlands) (equatorial forests)
Goualougo	Pollen	2.0875	16.54722	Brncic et al. (2007)	Central Africa (lowlands) (equatorial forests)
Lake Nguène	Pollen	−0.2	10.466	Ngomanda et al. (2007)	Central Africa (lowlands) (equatorial forests)
Lake Kamalété	Pollen	−0.7166	11.7666	Ngomanda et al. (2007)	Central Africa (lowlands) (equatorial forests)
Lake Sinnda	Pollen/sediment	−3.836111	12.8	Bertaux et al. (1998), Vincens et al. (1998)	Central Africa (lowlands) (equatorial forests)
Ngamakala	Pollen	−4.075	15.38333	Elenga (1992)	Central Africa (lowlands) (equatorial forests)
Lake Kitina	Pollen/sediment	−4.27	12	Bertaux et al. (1998), Elenga et al. (1996)	Central Africa (lowlands) (equatorial forests)
GeoB6518-1	Alkenone/ Geochemistry	−5.588333	11.221667	Schefuß et al. (2005)	Central Africa

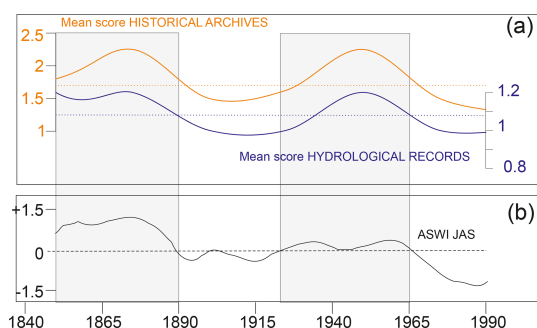


Figure 2. Observed and reconstructed rainfall anomalies over the Sahel during the 1840–1990 CE period. **(a)** The mean scores from historical (yellow curve) and natural archives (blue curve) for the Sahel (Nicholson, 1978, 1980, 2013; Nicholson et al., 2012; Coquery-Vidrovitch, 1997; Holmes et al., 1999; Street-Perrott et al., 2000; Waller et al., 2007; Wang et al., 2008; Multiza et al., 2010; Maley and Vernet, 2013; Lézine et al., 2019). The dotted yellow and blue lines correspond, respectively, to the historical and paleo-hydrological archive mean scores during the period 1850–1990 CE. They allow identifying anomalously wet and dry periods. **(b)** The African Southwesterly Index (ASWI) developed by Gallego et al. (2015) as a measure of rainfall anomalies in Sahel during the WAM rainy season (July to September).

precipitation amounts at a given site. Nevertheless, the curves are remarkably similar and point to wet periods centered on ca. 1875 and 1950 CE.

2.2 Model experiments

In this study we compare reconstructed environmental changes in Western Africa to those simulated in the past1000 model experiment covering the 850–1850 CE climate performed as part of fourth phase of the Paleoclimate Modelling Intercomparison Project (PMIP4; Jungclaus et al., 2017; Kageyama et al., 2017) by the IPSL-CM6A-LR model version developed for the Coupled Model Intercomparison Project phase 6 (CMIP6) at Institut Pierre-Simon Laplace (Boucher et al., 2020; Lurton et al., 2020). The IPSL-CM6A-LR model couples the atmospheric component LMDZ (Hourdin et al., 2020) to the land surface model ORCHIDEE (d’Orgeval et al., 2008) and to the ocean model NEMO, which includes other models to represent sea–ice interactions (Rousset et al., 2015) and biogeochemistry processes (Aumont et al., 2015). The atmospheric and land-surface grid have a resolution of 2.5° in longitude and 1.3° in latitude with 79 vertical layers. The oceanic component has 75 vertical levels with a mean spatial horizontal resolution of about 1° and a refinement of $1/3^\circ$ near the Equator. This model reproduces the ENSO seasonality fairly well (McPhaden et al., 2006) despite the sea surface temperature anomalies extending too far westward in the central Pacific during El Niño events. The spatial pattern of the Atlantic Multidecadal Variability (AMV; Deser et al., 2010)

teleconnection in the Pacific is consistent with observations, but the tropical Atlantic variability is relatively weaker. Unlike most current state-of-the-art CMIP6 models, the IPSL-CM6A-LR model simulates a predominant secular variability in the Atlantic with AMV peaks separated by about 200 years (Boucher et al., 2020).

The past1000 IPSL-CM6A-LR model experiment is designed to simulate the climate response to natural forcings recommended by PMIP4 (Jungclaus et al., 2017) and covering the pre-industrial millennium (850–1849 CE), namely time-varying astronomical parameters, trace gases (Meinshausen et al., 2017; Matthes et al., 2017), the eVolv2k volcanic forcing (Toohey and Sigl, 2017), the SATIRE-M 14C solar activity with an adaptation of the spectral irradiance to the CMIP6 *historical* forcing and the land use forcing (Lawrence et al., 2016). Three past1000 IPSL-CM6A-LR model simulations have been performed and branched off from various initial conditions in a 600-year-long spinup run with fixed external radiative forcing to the year 850 CE. This spinup run, itself branched off from the IPSL-CM6A-LR pre-industrial control (piControl) run with constant external radiative forcing, has been performed to avoid any spurious drift in the past 1000 experiments that could be related to the adjustment of the slow components of the climate system (such as the ocean) to the different radiative balance at the beginning of the last millennium as compared to the pre-industrial levels.

The IPSL-CM6A-LR model reproduces the observed climatological distribution of maximum rainfall across West Africa during the WAM rainy season (Fig. 3a). The timing of the simulated WAM seasonal cycle is also in good agreement with observations, with a well-defined onset of the rainy season in July and then a demise after September (Fig. 3b). However, the northward shift in maximum rainfall over the Sahel during the rainy season is underestimated by the model by about 4° (the model maximum in August is $\sim 7^\circ$ N and the observed one at 11° N). As a result the climatological rain belt over West Africa is slightly more constrained to tropical regions compared to observations and the dryer Sahel on average. However, the well-characterized WAM seasonal timing suggests that there are no remarkable biases affecting the simulated precipitation variability.

Then, to characterize the simulated Sahel rainfall multi-decadal variability over the past millennium and contrast it with the reconstructed environmental series, an index is calculated as the 10-year low-pass-filtered Sahel precipitation anomalies in the rainy season from the past1000 simulations. Seasonal precipitation anomalies from July to September (JAS), relatives of the piControl climatology, are area-weighted and averaged across the Sahel region (red box in Fig. 3a) and then filtered with a 10-year centered moving mean with truncated endpoints (i.e., only averaging existing elements within the 10-year window). An ensemble-mean index is also performed to highlight the forced component of the Sahel multidecadal variability in response to natural forc-

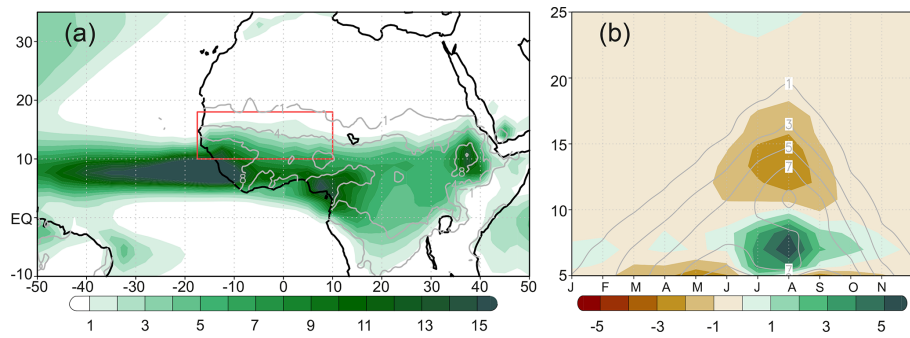


Figure 3. Climatological bias of simulated monthly precipitation. **(a)** JAS mean averaged across (colors) the 2000-year piControl run and (contours) the 1891–2019 period in the GPCPv2020 observational database. **(b)** Meridional seasonal cycle (colors) of the 10° W–10° E mean model bias (simulation minus observations) compared to (contours) the GPCPv2020 climatology. All units are millimeters per day. Red box in **(a)** indicates the Sahel region (10–18° N, 17.5° W–10° E).

ings that are common to the three past1000 members, such as the effect of large volcanic eruptions, in contrast to the internal variability.

3 Results

3.1 The hydrological records

The hydrological records provide a contrasting picture from one region to another: the Sahel, the Sudano-Guinean savannah zone and the tropical forests. They also reveal some local exceptions. As already noted (e.g., Vincens et al., 1999), the local hydrogeological context may strongly affect the individual response of lakes and wetlands to rainfall variations and partly explains this apparent heterogeneity.

The main characteristics of the hydrological evolution in the Sahel, in the savannah zone, and in low- and high-altitude equatorial forests can be summarized as follows (Fig. 4):

- Data from the central and western Sahel (Fig. 4a) point to a relatively dry period at the end of the first millennium (900 CE) at Bal, Kajemarum and in the Senegal River watershed (GeoB9501). A wet period followed, already present at Mboro near the littoral, which lasted up to 1350 CE. Except at Kajemarum and Jikariya, where hydrological conditions remained relatively stable, a gradual trend toward increased aridity is recorded in two steps dated ca. 1625 and 1800 CE, respectively. Then, during the last 2 centuries, only minor fluctuations occurred in a general context of widespread aridity.

In the Lake Chad area, Maley and Vernet (2013) depict a rather different and complex history probably due to the variety of the archives they used (both historical and natural) and also to the complexity of the hydrology of this immense waterbody (Pham-Duc et al., 2020) fed by underground waters and by rivers of distant geographical origin. The authors identify two major periods of

flooding in the Lake Chad area: from the onset of the millennium to ca. 1200 CE and then between 1600 and 1700 CE, with a series of dry periods in between, and then from 1700 CE onwards.

- Only three sites document the hydrological evolution of the savannah zone south of the Sahel (Fig. 4c). These sites are located in the center of the savannah zone (White, 1983): two crater lakes on the Adamawa plateaus (Mbalang and Tizong) and the other at the mouth of the tributary of Lake Petpenoun in the grass fields region of Cameroon. The Adamawa lakes do not show any significant hydrological changes throughout the last millennium. In contrast Petpenoun records a clear evolution towards aridity which started ca. 1425 CE and culminated in ca. 1650 CE.
- Diorom Boumak (Fig. 4b) is situated at the southern boundary of the Sahel, in the littoral mangroves of the Saloum estuary. In contrast to the other sites from the Sahel and savannah zone this site records a remarkable wet period between 1500 and 1800 CE. As elsewhere, however, aridification started ca. 1800 CE.
- The equatorial lowlands are characterized by contrasting hydrological situations reflecting the diversity of local hydrogeological settings (Fig. 4e). Low lake levels are recorded at Bosumtwi, Mopo Bai, Goulougo, Nguène–Kamalété and Ossa during a period centered around 1100 CE in contrast to Sinnda and Kitina, where moist conditions occurred. Moisture increased as soon as 1350 CE at Goulougo and continued up to 1400 CE at Mopo Bai and Kitina. Then, there is a clear opposition between Sinnda, Nguène–Kamalété and Bosumtwi, where low lake levels occurred during a dry phase between ca. 1350 and 1700 CE, and Mopo Bai, Goulougo, Ossa and Kitina, which are characterized by wetter conditions. In any case, the marine record at the mouth of the Congo River (GeoB6518-1) suggests

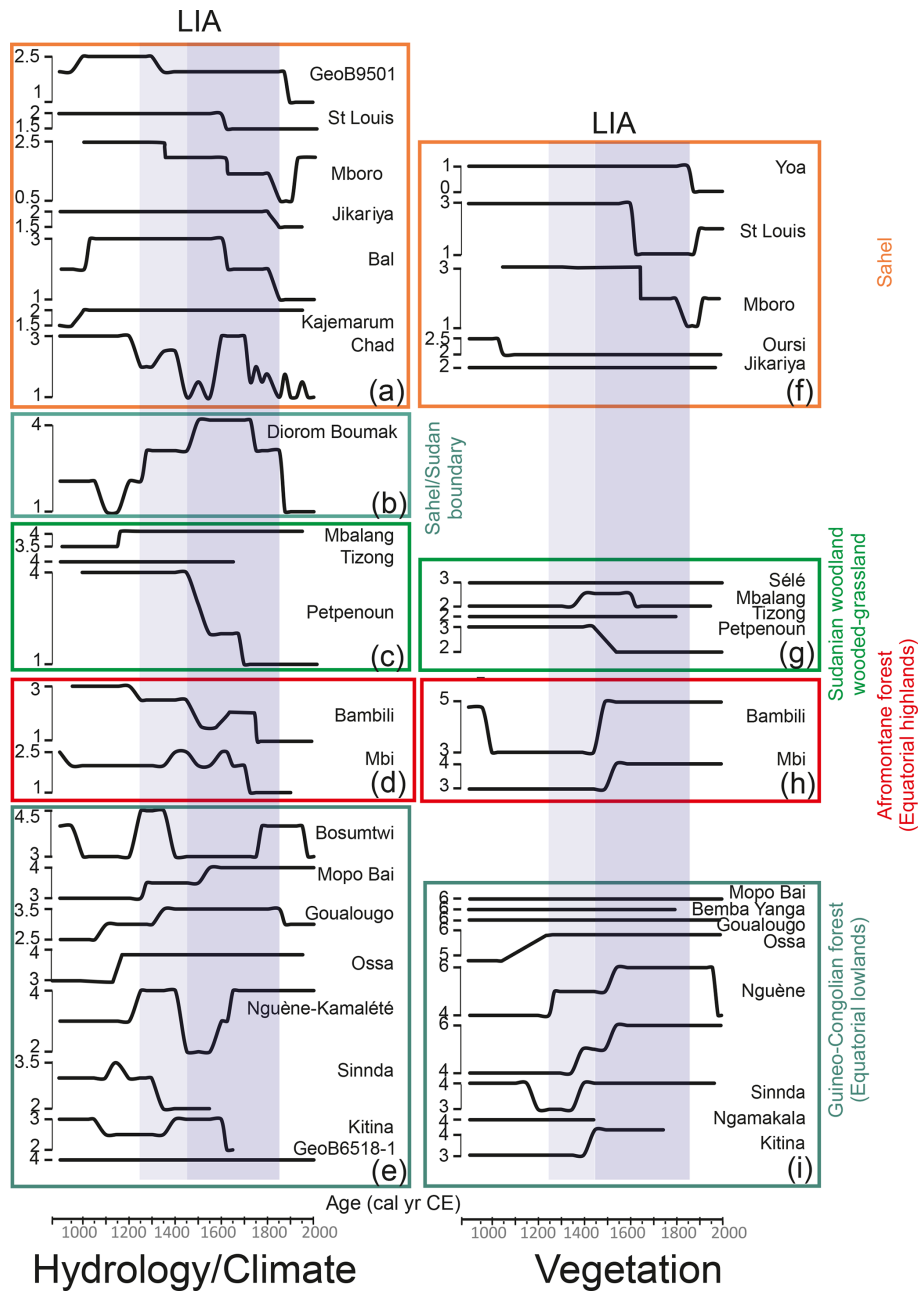


Figure 4. Mean scores of hydrological and vegetation changes along a north–south transect from the northern limit of the Sahel (Yoa) to the Congo Basin (GeoB6518-1). Data are grouped within the phytogeographical entities defined by White (1983) in tropical Africa: Sahelian grassland and wooded grassland, Sudano-Guinean savannah, highland Afromontane forest, and lowland Guineo-Congolian forest. The environmental index (bold black line) shows the evolution of vegetation from bare soil (0) to dense forest (6). The intermediate values are 1: steppe and grassland; 2: wooded grassland; 3: woodland and gallery forest; 4: degraded and secondary forest; 5: montane forest (f–i). For hydrology and climate, the index shows the evolution from dry (1) to wet (4) with intermediate values showing the gradation between these two extremes (a–e). The shaded vertical bands indicate the transition period between the Medieval Climate Anomaly and the Little Ice Age (1250–1450 CE, light shading) and the LIA (1450–1850 CE, dark shading).

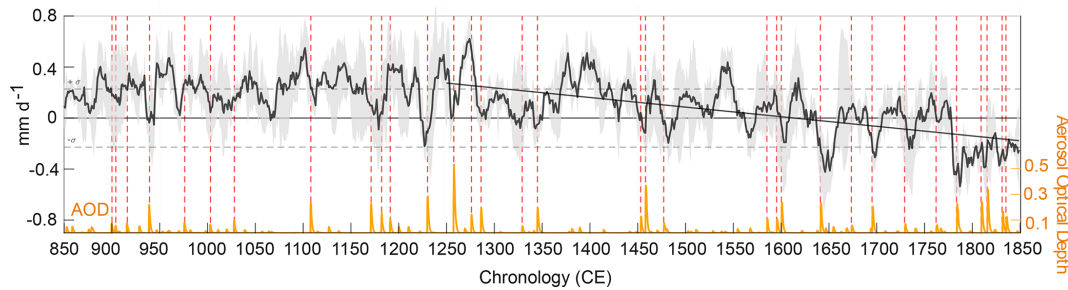


Figure 5. Multidecadal Sahel rainfall variability in IPSL-CM6A-LR past1000 simulations. Black line: 10-year low-pass-filtered index of Sahel JAS precipitation anomalies averaged in boxed area in Fig. 3 (i.e., 10–18° N and 17.5° W–10° E). The black line corresponds to the ensemble mean, the gray shading to the ensemble spread and the diagonal line to the 1250–1849 CE linear fit. Dashed horizontal lines show the \pm standard deviation of the equivalent piControl index. The volcanic forcing used in the IPSL-CM6A-LR model experiments is shown by the orange curve as the globally averaged aerosol optical depth (AOD). Red vertical dotted lines indicate the occurrence of strong volcanic eruptions about the size or larger than the Pinatubo eruption (June 1991) defined when the tropical (20° S–20° N) or northern extratropical (50–90° N) mean AOD is larger than 0.1.

that all these hydrological variations in the equatorial lowlands remained of relatively low amplitude.

- In the Cameroon highlands (Fig. 4d), hydrological conditions steadily declined as shown at Lake Bambili, starting from ca. 1250 and culminating ca. 1675 CE. This gradual trend is interrupted ca. 1500 CE by a more pronounced phase of lake level lowering. The Mbi swamp displays a rather different pattern: here, the water level was relatively low throughout the whole last millennium except in two discrete wetter phases ca. 1450 and 1650 CE.

3.2 Pollen data

- In the open landscapes of the Sahara, Sahel and savannah zones, vegetation changes were of minor amplitude except at sites where gallery forests were previously well developed. It is in the westernmost part of the Sahel that the most profound changes in vegetation cover are recorded: in the Niaye area (Mboro) and in the Senegal River delta (St Louis), the degradation of the landscape originated ca. 1300 CE and accelerated ca. 1600 CE to a maximum reached ca. 1850 CE (Fig. 4f). A discrete vegetation recovery is then recorded in the 19th century. In contrast, sites from the central Sahel (Oursi and Jikariya) remained relatively stable throughout the last millennium in spite of a slight degradation recorded at Oursi ca. 1050 CE. North of the Sahel (Yoa), the aridification of the desert landscape accelerated from the 19th century onward. South of the Sahel, in the savannah zone, lakes Tizong and Sélé do not record any marked environmental change contrary to Petpenoun, where a slight degradation is recorded ca. 1425 CE (Fig. 4g). At Mbalang, a discrete phase of vegetation recovery occurred between ca. 1400–1600 CE.

- The forest cover remained roughly unchanged in the central forest massif (Mopo Bai, Bemba Yanga, Goulougo, Fig. 4i). In the western regions by contrast, Ngamakala, Kitina, Lake Ossa, Nguène and Kamalété the forest gradually developed since 1250–1350 CE in spite of the discrete hydrological fluctuations. In the Cameroon highlands (Fig. 4h), the forest development occurred later, ca. 1550–1500 CE, after a phase of forest clearance from 1000 to 1450 CE.

3.3 Model results

The index of the ensemble-mean Sahel JAS precipitation simulated over the past millennium reveals a change from a relatively wet mean state in the MCA (950–1249 CE) to a drier one in the LIA (1450–1849) (Fig. 5), suggesting a shift in the average WAM rainfall regime. Such continuous decline presents a linear rate of the seasonal Sahel rainfall of -0.7 mm per decade over 1250–1849 CE, resulting in a 7 % loss of the mean precipitation in the LIA relative to MCA (Fig. 5). Regarding decadal variations, the ensemble-mean index of past1000 Sahel precipitation almost doubles its variability in the LIA with respect to the MCA (the variance in 859–1249 CE is 51 % higher than in 1450–1849 CE), which suggests a more unstable rainfall regime, apart from being drier on average, by the late past millennium in response to natural external forcings. Such a simulated long-term drying trend and increased LIA Sahel precipitation decadal variability is related to the volcanic forcing influence on SSTs, which integrates the induced radiative cooling (Fang et al., 2021). The more frequent large volcanic eruptions during the LIA, as compared to the MCA, are integrated by the ocean long memory, leading to a gradual SST decrease that is more pronounced in the Northern Hemisphere than the Southern Hemisphere. The relative North Atlantic SST cooling trend throughout 850–1849 CE gradually promotes a southward

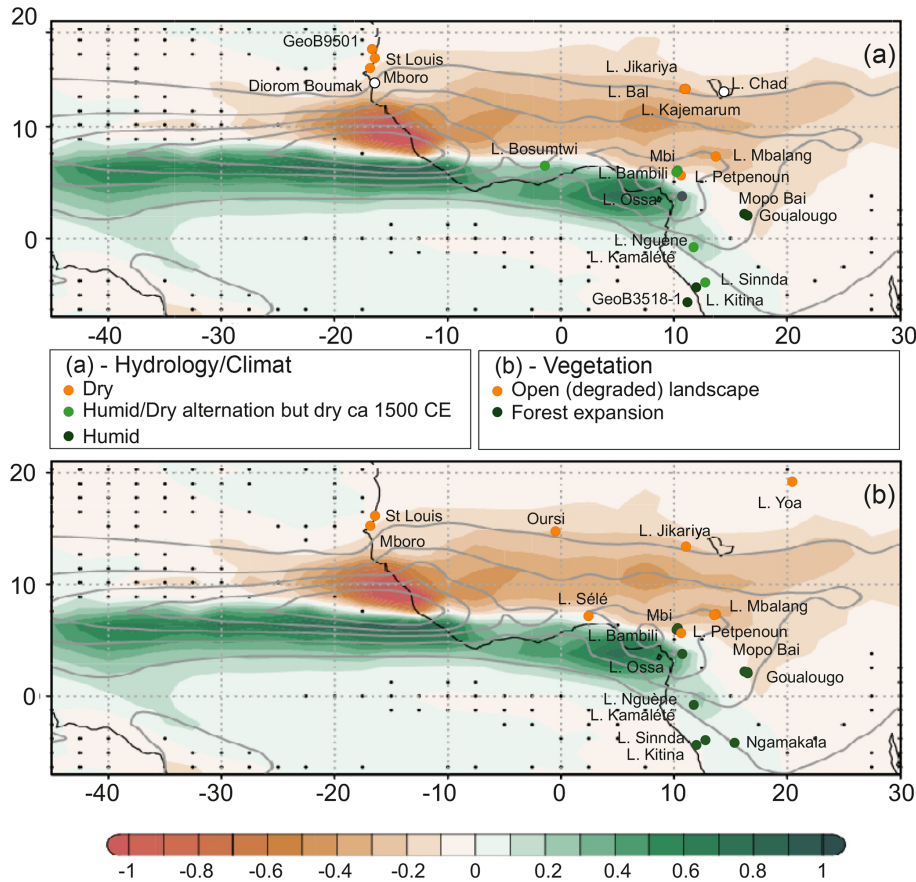


Figure 6. Distribution of JAS rainfall anomaly difference between the LIA (1450–1849 CE) and the MCA (950–1249 CE) as simulated by the IPSL-CM6A-LR model in the past1000 ensemble mean (shading, mm d^{-1}) compared to hydrological and dust (a) and vegetation (b) paleo-records during the LIA shown as dots following the same color scale as simulated anomalies. Gray contours indicate the piControl climatology from 2 mm d^{-1} in intervals of 4 mm d^{-1} . Stippling indicates disagreement across the three past1000 members on the sign of the represented difference.

shift in the Inter-Tropical Convergence Zone (ITCZ) and a weakening of monsoon moisture inflow to Western Africa. The long-term WAM weakening is further amplified in the few years following any new large volcanic event, occurrences of which are indicated by the vertical dotted lines in Fig. 5. As a consequence, more frequent negative rainfall anomalies lasting at least 5 consecutive years are also evident during the LIA as compared to the MCA, with significant drying that can persist up to 60 years around clusters of eruptions such as those of the 19th century.

4 Discussion

4.1 Hydrology and climate changes at a secular timescale

Data and past1000 model simulations show a strong north–south contrast between the Sahel and savannah zones, both subjected to severe drying during the LIA, and the equato-

rial areas, spanning the Gulf of Guinea coast, suggesting an overall change in the WAM.

The difference between the simulated past1000 JAS precipitation during the LIA and the MCA shows a characteristic distribution of a weakened WAM associated with a southward shift in the ITCZ, with less rainfall across the Sahel and more in the Gulf of Guinea coast (Fig. 6). These simulated anomalies are consistent with the overall distribution of hydrological and vegetation proxy reconstructions.

4.1.1 Hydrology

Three major regions can be recognized from the paleohydrological records: the Sahel and savannah zones, with a drying trend; the center of the Congo Basin, which exhibits an opposite trend of increasing humidity; and the boundary between the dry and humid domains defined by the equatorial sectors closest to the coast or in mountains, where an alternation of wet and dry phases is recorded. Two paleo-records differ from this general picture: that of Lake Chad,

where a period of flooding is recorded ca 1600 CE and that of the Diorom Boumak, where the LIA is entirely characterized by a wet period (Fig. 4). As evoked above, the multiple origins of the data and the complex hydrological system of Lake Chad may have introduced a bias into the hydrological record and may explain (at least partly) the difference with the other Sahelian archives. It is also likely that the rivers that feed the lake, which originate from southern regions (the Chari and Logone rivers and their tributaries), may have caused an influx of water during the short humid phase recorded on the Cameroon highlands (Bambili and Mbi) ca. 1600 CE. The case of the Diorom Boumak site is more complex: the historical records mentioned by Maley and Vernet (2013) or Carré et al. (2019), among others, indicate that the Saloum sector was wetter than the rest of the Sahel during part of the 16th century, allowing for the establishment of two harvests per year. According to Maley and Vernet (2013), this may have been due to the occurrence of two rainy seasons: one in the core of the WAM season in summer and another (usually of lesser importance) referred to as “heug rains” linked to polar air intrusions in winter (Le Borgne, 1979).

4.1.2 Vegetation

In the central Sahel, already degraded prior to the LIA (Lézine et al., 2021), such as at Oursi, no significant change occurred in the vegetation landscape, which remained open throughout the last millennium (Fig. 4b). The same pattern is observed in the wettest areas of the Congo Basin, where the forests remained unchanged in composition and physiognomy (Tovar et al., 2019). Elsewhere in the forest galleries of the Sahel and the savannah zone (Mboro, St Louis, Petpenoun) the evolution of vegetation mirrored that of hydrological conditions while recording a gradual degradation that culminated around 1800–1850 CE. In the westernmost sector of the Sahel (Mboro, St Louis), the data suggest, however, a slight recovery of the vegetation cover during the last few decades.

In contrast, both high- and low-elevation sites from the equatorial forest regions show an opposite trend with marked forest recovery that began in the early years of the LIA and accelerated around 1450 CE. The forest expanded in the equatorial lowlands despite increased human presence, which has already been noted by Vincens et al. (1999). That means that the local hydrological variations, and particularly the 1500 CE dry event, were of too small an amplitude to impact forest dynamics. At most, a plateau in forest recovery is observed at that time (Nguène, Kamalété). While the forest recovery was gradual at low altitudes, it seems to have occurred more abruptly in the highlands.

4.2 The chronology of events at a multidecadal timescale: focus on the Sahel and savannah zone

Environmental changes in the Sahel and savannah zones during the LIA occurred in the context of widespread environmental degradation that followed the severe environmental crisis at the end of the African Humid Period (AHP; Demenocal et al., 2000). Between 3300 and 2500 cal yr BP (Lézine et al., 2021), the forests and woodlands, which expanded widely across the plains and mountains of West Africa, strongly declined. This is particularly striking along the Atlantic coast of Senegal, between 15 and 17° N, where specific environmental conditions related to the proximity of the sea and the presence of a water table near the surface favored the development of exceptionally dense forest galleries of humid tropical affinity during the AHP (Lézine, 1989). As a result of this major environmental crisis, the Sahel and savannah zone took on its modern aspect of semi-desert grassland and wooded grassland. In this context, discernible environmental fluctuations, particularly in vegetation, are of limited magnitude, with the exception of sectors where forest galleries were widely established during the AHP.

To discuss the chronology of events that punctuated the LIA, paleo-data were averaged in each geographical area (Sahel, savannah zone) in the two categories covered by our study: hydrology and climate and vegetation (Fig. 7a). A Drying Persistence Index was constructed from our model results in order to quantify the Sahel precipitation deficit over at least 50-year periods (red curve in Fig. 7b). It is defined at each year as the negative linear trend of the Sahel ensemble-mean JAS precipitation (black curve in Fig. 7b) across the 50 previous years. We use 50 years to be consistent with the multidecadal to centennial temporal resolution of the paleo-data.

The past1000 simulations represent several drying events of various amplitude and duration during the MCA that do not correspond to any major change in the vegetation of the Sahel and savannah zone. Instead, the environment in these two areas appears to be characterized by a relatively stable humid regime (Fig. 7a). This is coherent with the rainy mean state represented by the past1000 simulations over the MCA, which is associated with an anomalous northward ITCZ position (green curve in Fig. 7b) throughout all of this period compared to the LIA.

At the end of the MCA, two early warning signals (Lenton, 2011) of Sahel drying events centered at 1170 and 1240 CE are identified in our model experiments. The intensity and brevity of these two events contrast with the minor dry phases identified prior to the LIA since the onset of the last millennium. The Drying Persistence Index at these two events, the timing of which coincides with the occurrence of large clusters of volcanic eruptions (orange curve Fig. 7b), reaches over -0.3 mm d^{-1} across 50 years. Both events preceded the onset of the LIA gradual drying trend starting at 1250 CE. This drying trend was sustained by the southward migration

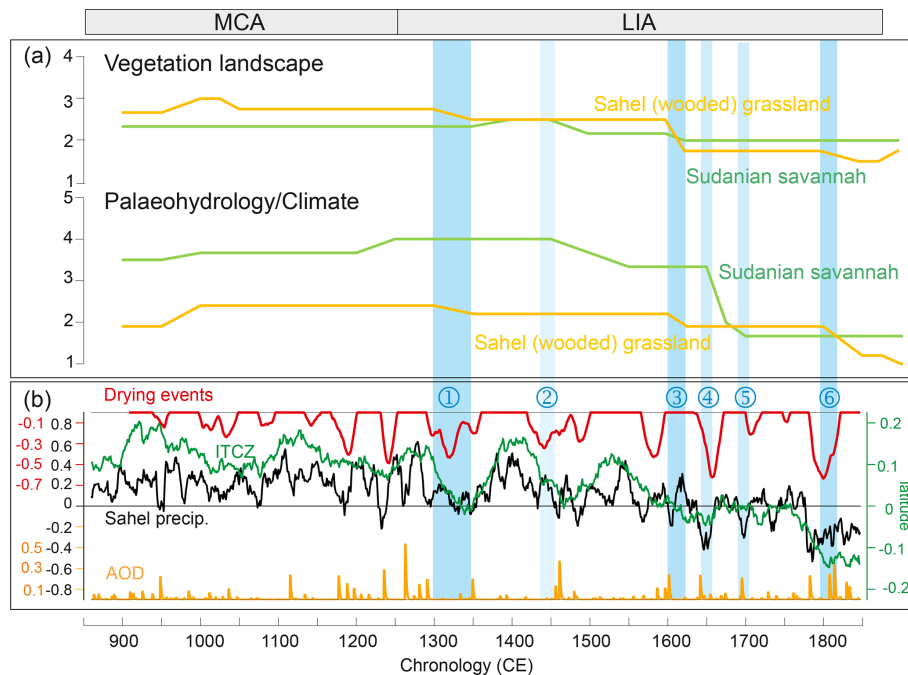


Figure 7. Multiproxy records of hydrology and vegetation during the last millennium in the driest biomes (Sahel and savannah zone) in western Africa (a) and long-term evolution of rainfall over the Sahel as simulated by the IPSL-CM6A-LR past1000 model (b). Panel (b): 10-year filtered ensemble-mean Sahel precipitation index (mm d^{-1}) (black line); 50-year filtered anomalous latitudinal position of the JAS ITCZ (defined as the latitudinal maximum zonal-mean rainfall in 40°W – 10°E) in the past1000 simulations to the piControl JAS mean position (in degrees of latitude) (green line); global-mean AOD (volcanic forcing) (orange line); Sahel Drying Persistence Index defined as the 50-year running negative trend values over the Sahel ensemble-mean JAS precipitation index (mm d^{-1} per 50 years) (red line). Blue bars and numbers highlight the main climate and environmental degradation thresholds identified in the paleo-records.

of the ITCZ, which shifts south of the piControl mean position at 1600 CE. It is consistent with the continuous degradation of hydrological and vegetation conditions since 1250 CE in the Sahel and savannah zone identified in our multiproxy records.

Several abrupt drying events larger than those identified during the MCA punctuated the LIA, some of which reached over -0.5 mm d^{-1} across 50 years. Despite the difference in temporal scale between the two approaches used here, there is a striking agreement between the major simulated droughts and the environmental degradation steps in our paleo-records (blue bars in Fig. 7). These degradation periods, in turn, span the largest eruptions from ca. 1250 to ca. 1850 CE, which are associated with the multidecadal variability of Sahel precipitation over the past millennium in PMIP4 multi-model experiments.

4.2.1 Steps in the degradation of the climate and the environment in the Sahel

Three major steps are identified:

- The first dramatic environmental degradation occurred between 1290 and 1350 CE (event 1), i.e., ca. 50 years after the first warning signal and lasted about 60 years.

Dust fluxes to the ocean, which had stabilized during the Medieval Warm Period, increased (Mulitza et al., 2010) whereas lake levels dropped in the interdunal depressions in the western Sahel leading to the salinization of the waters (Lézine et al., 2019).

- The second stage in the degradation of environmental conditions occurred ca. 1600 CE (event 3). The environmental degradation was common to the entire Sahel (Bal, Mboro, St-Louis) while corresponding to a major collapse of the forest galleries at Mboro. Here also, a time lag of ca. 50 years can be observed between the onset of a drought phase and the response of the vegetation.
- The ultimate environmental threshold is recorded ca. 1800 CE (event 6). It resulted in the widespread lowering of lake levels, the massive contribution of dust to the ocean and the irreversible destruction of forest galleries in the western Sahel in response to an abrupt drop in rainfall ca. 1800 CE, already observed by Carré et al. (2019) in the Saloum River delta. By accounting for a catastrophic decrease in precipitation of -0.6 mm d^{-1} over 50 years in our model experiments, this climatic tipping point, related to closely spaced

large volcanic eruptions (starting with the Laki eruption in 1783 CE followed by the eruptions cluster over the 1809–1835 CE period including the 1815 Tambora event), at the origin of the modern environmental conditions in the Sahel, was twice as large as the early warning signals identified at the end of the MCA.

Our data–model comparison suggests that there was a time lag of several decades (typically 50 years) between the climate signal and the environmental response. If this time lag is highly probable, its duration and origin require further investigation. It may indeed result from the resilience of plants to climate change, but we cannot exclude the memory effect of aquifers already observed by Aguiar et al. (2010) that may induce a delay between the climate signal and its effects on ecosystems. The uncertainty associated with the ages, whether it comes from the data or from the modeling, can also play a role by increasing or reducing this response time.

4.2.2 The savannah zone

As the ITCZ moved to more southerly latitudes, some of the drought events reconstructed in the Sahel had a major impact in the savannah zone. Here, data are particularly sparse and, as in the Sahel, changes in vegetation are hardly distinguishable in these already highly degraded environments, such as at Lake Sélé (Salzmann and Hoelzmann, 2005). It is at Lake Petpenoun (Catrain, 2021) that the evidence is the clearest due to the presence of a gallery forest and pronounced hydrological changes at the core site.

We find that the last step of degradation of the savannah vegetation occurred during event 3 also observed in the Sahel. Events 2 (1447–1493 CE), 4 (1643–1657 CE) and 5 (1691–1707 CE) correspond only to phases of hydrological degradation that are not reflected in the regional vegetation. Data are still too rare to generalize this observation to the entire savannah zone and could only account for local conditions.

5 Conclusion

Despite the uncertainties associated with data scarcity and heterogeneity, our study shows a remarkable agreement between the data and our past1000 model experiments for reconstructing the climate and environmental changes in response to natural forcing that characterized the LIA in western Africa. It highlights a north–south contrast between the dryness of the Sahel and the humidity of the equatorial zone. Despite the major difficulty related to the type of vegetation at play in the Sahel and the savannah zone already degraded since the end of the AHP, major steps in the degradation of the environment can be identified. Our most remarkable results consist of (1) the identification of two early warning signals at 1170 and 1240 CE, i.e., prior to the progressive

LIA drying of the Sahel that led to the climatic tipping point at 1800–1850 CE. This tipping point marks the setting in of arid conditions (the driest condition since 850 CE) which still persist today; (2) the identification of abrupt drought events which punctuated the LIA, the most important of which impacted both the Sahel and the savannah zone ca. 1600 CE. The consistency between proxy records and our model experiments suggests a strong role of large volcanic eruptions in shaping Sahel environmental changes over the pre-industrial millennium. Further work relying on large ensembles of climate and vegetation models will help assess such hypotheses.

Code availability. The IPSL-CM6A-LR model code used in this work was frozen (version 6.1.0) and subsequently altered only for correcting diagnostics or allowing further options and configurations. Versions 6.1.0 to 6.1.11 are therefore bit-reproducible for a given domain decomposition, compiling options and supercomputer. LMDZ, XIOS, NEMO and ORCHIDEE are released under the terms of the CeCILL license. OASIS-MCT is released under the terms of the Lesser GNU General Public License (LGPL). The IPSL-CM6A-LR code (version 6.1.11) is publicly available through the following direct link: <https://doi.org/10.14768/35339a29-61e8-4dea-9f8e-1c40f5699d99> (Boucher et al., 2023). The mod.def file provides information regarding the different revisions used, namely (1) NEMOGCM branch nemov36STABLE revision 9455; (2) XIOS2 branches/xios-2.5 revision 1873; (3) IOIP-SL/src svn tags/v224; (4) LMDZ6 branches/IPSLCM6.0.15 rev 3643; (5) tags/ORCHIDEE20/ORCHIDEE revision 6592; and (6) OASIS3-MCT 2.0branch (rev 4775 IPSL server). We recommend referring to the project website, http://forge.ipsl.jussieu.fr/igcmg_doc/wiki/Doc/Config/IPSLCM6 (IGCMG, 2023), for proper installation and compilation of the environment (version 6.1.10).

Data availability. Pollen data are available on the African Pollen Database website: <https://africanpollendatabase.ipsl.fr> (African Pollen Database, 2023). The other paleo-data are from the literature.

The IPSL-CM6A-LR model data and pre-processed model and proxy data sets used in this study are available at <https://doi.org/10.5281/zenodo.7003853> (Lézine et al., 2022).

Supplement. The supplement related to this article is available online at: <https://doi.org/10.5194/cp-19-277-2023-supplement>.

Author contributions. AML and MK designed the study. MK performed the IPSL-CM6A-LR model past1000 simulations and JV the simulation analysis. MC and AML collected and analyzed the data. AML prepared the paper with contributions from all co-authors.

Competing interests. The contact author has declared that none of the authors has any competing interests.

Disclaimer. Publisher’s note: Copernicus Publications remains neutral with regard to jurisdictional claims in published maps and institutional affiliations.

Acknowledgements. This work contributes to the ACCEDE ANR Belmont Forum project (18 BELM 0001 05). This work was undertaken in the framework of the French L-IPSL LABEX and the IPSL Climate Graduate School EUR and benefited from the FNS “SYNERGIA EffeCts of lArge voLcanic eruptions on climate and societies: UnDerstanding impacts of past Events and related subsidence cRises to evaluate potential risks in the future” (CALDERA) project under French CNRS grant agreement number CRSII5_183571 – CALDERA. Myriam Khodri acknowledges support from the HPC resources of TGCC under the allocations 2020-A0080107732 and 2021-A0100107732 (project genchip6) provided by GENCI (Grand Equipement National de Calcul Intensif) and 2020225424 provided by PRACE (Partnership for Advanced Computing in Europe). This study benefited from the ESPRI computing and data center (<https://mesocentre.ipsl.fr>, last access: 24 January 2023), which is supported by CNRS, Sorbonne Université, Ecole Polytechnique and CNES as well as through national and international grants. Thanks are due to the African Pollen Database for data access. Anne-Marie Lézine, Maé Catrain and Julián Villamayor were funded by CNRS and Myriam Khodri by IRD. We acknowledge the World Climate Research Programme’s Working Group on Coupled Modelling.

Financial support. This research has been supported by the Agence Nationale de la Recherche (grant no. 18 BELM 0001 05).

Review statement. This paper was edited by Hugues Goosse and reviewed by two anonymous referees.

References

- African Pollen Database: Welcome to the new African Pollen Database web site, <https://africanpollendatabase.ipsl.fr>, last access: 24 January 2023.
- Aguiar, L., Garneau, M., Lézine, A.-M., and Maugis, P.: Evolution de la nappe des sables quaternaires dans la région des Niayes du Sénégal (1958–1994): relation avec le climat et les impacts anthropiques, *Sécheresse*, 21, 1–8, <https://doi.org/10.1684/sec.2010.0237>, 2010.
- Aumont, O., Éthé, C., Tagliabue, A., Bopp, L., and Gehlen, M.: PISCES-v2: an ocean biogeochemical model for carbon and ecosystem studies, *Geosci. Model Dev.*, 8, 2465–2513, <https://doi.org/10.5194/gmd-8-2465-2015>, 2015.
- Ballouche, A.: Dynamique des paysages végétaux sahélo-soudaniens et pratiques agro-pastorales à l’Holocène : exemples au Burkina Faso, *Bull. Asso. Géogr. Français*, 75, 191–200, 1998.
- Bertaux, J., Sifeddine, A., Schwartz, D., Vincens, A., and Elenga, H.: Enregistrement sédimentologique de la phase sèche d’Afrique Equatoriale c. 3000 BP par la spectrométrie IR dans les lacs Sinnda et Kitina (Sud Congo), in: *Dynamique à long terme des écosystèmes forestiers intertropicaux*, ORSTOM, Paris, 213–215, ISBN 92-3-203753-X, 1998.
- Boucher, O., Servonnat, J., Albright, A.L., Aumont, O., Balkanski, Y., Bastrikov, V., Bekki, S., Bonnet, R., Bony, S., Bopp, L., Braconnot, P., Brockmann, P., Cadule, P., Caubel, A., Cheruy, F., Codron, F., Cozic, A., Cugnet, D., D’Andrea, F., Davini, P., de Lavergne, C., Denvil, S., Deshayes, J., Devilliers, M., Ducharne, A., Dufresne, J. L., Dupont, E., Éthé, C., Fairhead, L., Falletti, L., Flavoni, S., Foujols, M. A., Gardoll, S., Gastineau, G., Ghattas, J., Grandpeix, J. Y., Guenet, B., Guez, L. E., Guilyardi, E., Guimberteau, M., Hauglustaine, D., Hourdin, F., Idelkadi, A., Joussaume, S., Kageyama, M., Khodri, M., Krinner, G., Lebas, N., Levvasseur, G., Lévy, C., Li, L., Lott, F., Lurton, T., Luyssaert, S., Madec, G., Madeleine, J. B., Maignan, F., Marchand, M., Marti, O., Mellul, L., Meurdesoif, Y., Mignot, J., Musat, I., Ottlé, C., Peylin, P., Planton, Y., Polcher, J., Rio, C., Rochetin, N., Rousset, C., Sepulchre, P., Sima, A., Swingedouw, D., Thiéblemont, R., Traore, A. K., Vancoppenolle, M., Vial, J., Vialard, J., Viovy, N., and Vuichard, N.: Presentation and evaluation of the IPSL-CM6A-LR climate model, *J. Adv. Model. Earth Syst.*, 12, e2019MS002010, <https://doi.org/10.1029/2019MS002010>, 2020.
- Boucher, O., Servonnat, J., Albright, A. L., Aumont, O., Balkanski, Y., Bastrikov, V., Bekki, S., Bonnet, R., Bony, S., Bopp, L., Braconnot, P., Brockmann, P., Cadule, P., Caubel, A., Cheruy, F., Codron, F., Cozic, A., Cugnet, D., D’Andrea, F., Davini, P., de Lavergne, C., Denvil, S., Deshayes, J., Devilliers, M., Ducharne, A., Dufresne, J. L., Dupont, E., Éthé, C., Fairhead, L., Falletti, L., Flavoni, S., Foujols, M. A., Gardoll, S., Gastineau, G., Ghattas, J., Grandpeix, J. Y., Guenet, B., Guez, L. E., Guilyardi, E., Guimberteau, M., Hauglustaine, D., Hourdin, F., Idelkadi, A., Joussaume, S., Kageyama, M., Khodri, M., Krinner, G., Lebas, N., Levvasseur, G., Lévy, C., Li, L., Lott, F., Lurton, T., Luyssaert, S., Madec, G., Madeleine, J. B., Maignan, F., Marchand, M., Marti, O., Mellul, L., Meurdesoif, Y., Mignot, J., Musat, I., Ottlé, C., Peylin, P., Planton, Y., Polcher, J., Rio, C., Rochetin, N., Rousset, C., Sepulchre, P., Sima, A., Swingedouw, D., Thiéblemont, R., Traore, A. K., Vancoppenolle, M., Vial, J., Vialard, J., Viovy, N., and Vuichard, N.: Presentation and evaluation of the IPSL-CM6A-LR climate model, *IPSL [code]*, <https://doi.org/10.14768/35339a29-61e8-4dea-9f8e-1c40f5699d99>, 2023.
- Brcic, T. M., Willis, K. J., Harris, D. J., and Washington, R.: Culture or climate? The relative influences of past processes on the composition of the lowland Congo rainforest, *Philos. T. Roy. Soc. B*, 362, 229–242, <https://doi.org/10.1098/rstb.2006.1982>, 2007.
- Brcic, T. M., Willis, K. J., Harris, D. J., Telfer, M. W., and Bailey, R. M.: Fire and climate change impacts on lowland forest composition in northern Congo during the last 2580 years from palaeoecological analyses of a seasonally flooded swamp, *Holocene*, 19, 79–89, <https://doi.org/10.1177/0959683608098954>, 2009.
- Carré, M., Azzoug, M., Zaharias, P., Camara, A., Cheddadi, R., Chevalier, M., Fiorillo, D., Gaye, A. T., Janicot, S., Khodri, M., Lazar, A., Lazareth, C. E., Mignot, J., Mitma Garcia, N., Patris, N., Perrot, O., and Wade, M.: Modern drought conditions in western Sahel unprecedented in the past 1600 years, *Clim. Dy-*

- nam., 52, 1949–1964, <https://doi.org/10.1007/s00382-018-4311-3>, 2019.
- Catrain, M.: Le Petit Age de Glace en Afrique équatoriale: apport de l'étude palynologique des sédiments du lac de Petpenoun, Cameroun, Unpublished MS Thesis, University of Paris Saclay, 2021.
- Coquery-Vidrovitch, C.: Écologie et histoire en Afrique noire, Histoire, économie et société, 483–504, <https://www.jstor.org/stable/23612564> (last access: 24 January 2023), 1997.
- Demenocal, P., Ortiz, J., Guilderson, T., Adkins, J., Sarnthein, M., Baker, L., and Yarusinsky, M.: Abrupt onset and termination of the African Humid Period: rapid climate responses to gradual insolation forcing, *Quaternary Sci. Rev.*, 19, 347–361, [https://doi.org/10.1016/S0277-3791\(99\)00081-5](https://doi.org/10.1016/S0277-3791(99)00081-5), 2000.
- Descroix, L., Diogue Niang, A., Panthou, G., Bosdian, A., Sane, Y., Dacosta, H., Malam Abdou, M., Vandervaere, J. P., and Quantin, G.: Evolution récente de la pluviométrie en Afrique de l'Ouest à travers deux régions: la Sénégambie et le bassin du Niger moyen, *Climatologie*, 12, 25–43, 2015.
- Deser, C., Alexander, M. A., Xie, S. P., and Phillips, A. S.: Sea surface temperature variability: Patterns and mechanisms, *Annu. Rev. Mar. Sci.*, 2, 115–143, <https://doi.org/10.1146/annurev-marine-120408-151453>, 2010.
- d'Orgeval, T., Polcher, J., and de Rosnay, P.: Sensitivity of the West African hydrological cycle in ORCHIDEE to infiltration processes, *Hydrol. Earth Syst. Sci.*, 12, 1387–1401, <https://doi.org/10.5194/hess-12-1387-2008>, 2008.
- Elenga, H.: Végétation et climat du Congo depuis 24 000 ans B.P.: analyse palynologique de séquences sédimentaires du Pays Bateke et du littoral, PhD Thesis, Aix-Marseille III, 1992.
- Elenga, H., Schwartz, D., Vincens, A., Bertaux, J., de Namur, C., Martin, L., Wirmann, D., and Servant, M.: Diagramme pollinique holocène du lac Kitina (Congo): mise en évidence de changements paléobotaniques et paléoclimatiques dans le massif forestier du Mayombe, *Série 2a, C. R. Acad. Sci.*, 323, 403–410, 1996.
- Fang, S. W., Khodri, M., Timmreck, C., Zanchettin, D., and Jungclaus, J.: Disentangling internal and external contributions to Atlantic multidecadal variability over the past millennium, *Geophys. Res. Lett.*, 48, e2021GL095990, <https://doi.org/10.1029/2021GL095990>, 2021.
- Fofana, C. A. K., Sow, E., and Lézine, A.-M.: The Senegal River during the last millennium, *Rev. Palaeobot. Palynol.*, 275, 104175, <https://doi.org/10.1016/j.revpalbo.2020.104175>, 2020.
- Folland, C. K., Palmer, T. N., and Parker, D. E.: Sahel rainfall and worldwide sea temperatures, 1901–85, *Nature*, 320, 602–607, <https://doi.org/10.1038/320602a0>, 1986.
- Gadgil, S.: The monsoon system: Land–sea breeze or the ITCZ?, *J. Earth Syst. Sci.*, 127, 1, <https://doi.org/10.1007/s12040-017-0916-x>, 2018.
- Gallego, D., Ordóñez, P., Ribera, P., Peña-Ortiz, C., and García-Herrera, R.: An instrumental index of the West African Monsoon back to the nineteenth century, *Q. J. Roy. Meteorol. Soc.*, 141, 3166–3176, <https://doi.org/10.1002/qj.2601>, 2015.
- Giannini, A., Saravanan, R., and Chang, P.: Oceanic forcing of Sahel rainfall on interannual to interdecadal time scales, *Science*, 302, 1027–1030, <https://doi.org/10.1126/science.1089357>, 2003.
- Holmes, J. A., Allen, M. J., Street-Perrott, F. A., Ivanovich, M., Perrott, R. A., and Waller, M. P.: Late Holocene palaeolimnology of Bal Lake, northern Nigeria, a multidisciplinary study, *Palaeogeogr. Palaeoclimatol.*, 148, 169–185, [https://doi.org/10.1016/S0031-0182\(98\)00182-5](https://doi.org/10.1016/S0031-0182(98)00182-5), 1999.
- Hourdin, F., Rio, C., Grandpeix, J. Y., Madeleine, J. B., Cheruy, F., Rochetin, N., Jam, A., Musat, I., Idelkadi, A., Fairhead, L., Foujols, M. A., Mellul, L., Traore, A. K., Dufresne, J. L., Boucher, O., Lefebvre, M. P., Millour, E., Vignon, E., Jouhaud, J., Diallo, F. B., Lott, F., Gastineau, G., Caubel, A., Meurdesoif, Y., and Ghattas, J.: LMDZ6A: the atmospheric component of the IPSL climate model with improved and better tuned physics, *J. Adv. Model. Earth Syst.*, 12, e2019MS001892, <https://doi.org/10.1029/2019MS001892>, 2020.
- IGCMG: IPSLCM6 configuration, http://forge.ipsl.jussieu.fr/igcmg_doc/wiki/Doc/Config/IPSLCM6, last access: 24 January 2023.
- Jungclaus, J. H., Bard, E., Baroni, M., Braconnot, P., Cao, J., Chini, L. P., Egorova, T., Evans, M., Gonzalez-Rouco, J. F., Goose, H., Hurtt, G. C., Joos, F., Kaplan, J. O., Khodri, M., Goldewijk, K. K., Krivova, N., LeGrance, A. N., Lorenz, S. J., Luterbacher, J., Man, W., Maucock, A. C., Mainshausen, M., Moberg, A., Muscheler, R., Nehbass-Ahles, C., Otto-Bliesner, B. I., Phipps, S. J., Pongratz, J., Rozanov, E., Schmidt, G. A., Schmidt, H., Schmutz, W., Schurer, A., Shapiro, A. I., Sigl, M., Smerdon, J. E., Solanki, S. K., Timmreck, C., Toohey, M., Usoskin, I. G., Wagner, S., Wu, C. J., Yeo, K. L., Zanchettin, D., Zhang, Q., and Zorita, E.: The PMIP4 contribution to CMIP6 – Part 3: The last millennium, scientific objective, and experimental design for the PMIP4 past1000 simulations, *Geosci. Model Dev.*, 10, 4005–4033, <https://doi.org/10.5194/gmd-10-4005-2017>, 2017.
- Kageyama, M., Albani, S., Braconnot, P., Harrison, S. P., Hopcroft, P. O., Ivanovic, R. F., Lambert, F., Marti, O., Peltier, W. R., Peterschmitt, J. Y., Roche, D. M., Tarasov, L., Zhang, X., Brady, E. C., Haywood, A. M., LeGrande, A. N., Lunt, D. J., Mahowald, N. M., Mikolajewicz, U., Nisancioglu, K. H., Otto-Bliesner, B. L., Renssen, H., Tomas, R. A., Zhang, Q., Abe-Ouchi, A., Bartlein, P. J., Cao, J., Li, Q., Lohmann, G., Ohgaito, R., Shi, X., Volodin, E., Yoshida, K., Zhang, X., and Zheng, W.: The PMIP4 contribution to CMIP6 – Part 4: Scientific objectives and experimental design of the PMIP4-CMIP6 Last Glacial Maximum experiments and PMIP4 sensitivity experiments, *Geosci. Model Dev.*, 10, 4035–4055, <https://doi.org/10.5194/gmd-10-4035-2017>, 2017.
- Kanamitsu, M., Ebisuzaki, W., Woollen, J., Yang, S.-K., Hnilo, J. J., Fiorino, M., and Potter, G. L.: NCEP-DOE AMIP-II Reanalysis (R-2), *B. Am. Meteorol. Soc.*, 83, 1631–1643, <https://doi.org/10.1175/BAMS-83-11-1631>, 2002.
- Kucharski, F., Molteni, F., King, M. P., Farneti, R., Kang, I. S., and Feudale, L.: On the need of intermediate complexity general circulation models: A “SPEEDY” example, *B. Am. Meteorol. Soc.*, 94, 25–30, <https://doi.org/10.1175/BAMS-D-11-00238.1>, 2013.
- Lawrence, D. M., Hurtt, G. C., Arneth, A., Brovkin, V., Calvin, K. V., Jones, A. D., Jones, C. D., Lawrence, P. J., de Noblet-Ducoudré, N., Pongratz, J., Seneviratne, S. I., and Shevliakova, E.: The Land Use Model Intercomparison Project (LUMIP) contribution to CMIP6: rationale and experimental design, *Geosci. Model Dev.*, 9, 2973–2998, <https://doi.org/10.5194/gmd-9-2973-2016>, 2016.
- Lebamba, J., Vincens, A., Lézine, A.-M., Marchant, R., and Buchet, G.: Forest-savannah dynamics on the Adamawa plateau (Central Cameroon) during the “African humid pe-

- riod” termination: A new high-resolution pollen record from Lake Tizong, *Rev. Palaeobot. Palynol.*, 235, 129–139, <https://doi.org/10.1016/j.revpalbo.2016.10.001>, 2016.
- Le Borgne, J.: Un exemple d’invasion polaire sur la région mauritano-sénégalaise, *Ann. Géogr.*, 489, 521–548, 1979.
- Lenton, T. M.: Early warning of climate tipping points, *Nat. Clim. Change*, 1, 201–209, <https://doi.org/10.1038/nclimate1143>, 2011.
- Lézine, A. M.: Late Quaternary vegetation and climate of the Sahel, *Quatern. Res.*, 32, 317–334, [https://doi.org/10.1016/0033-5894\(89\)90098-7](https://doi.org/10.1016/0033-5894(89)90098-7), 1989.
- Lézine, A. M., Zheng, W., Braconnot, P., and Krinner, G.: Late Holocene plant and climate evolution at Lake Yoa, northern Chad: pollen data and climate simulations, *Clim. Past*, 7, 1351–1362, <https://doi.org/10.5194/cp-7-1351-2011>, 2011.
- Lézine, A. M., Holl, A., Lebamba, J., Vincens, A., Assi-Khaudjis, C., Février, L., and Sultan, E.: Temporal relationship between Holocene human occupation and vegetation change along the northwestern margin of the Central African rainforest, *C. R. Géosci.*, 345, 327–335, <https://doi.org/10.1016/j.crte.2013.03.001>, 2013.
- Lézine, A. M., Lemonnier, K., and Fofana, C. A. K.: Sahel environmental variability during the last millennium: insight from a pollen, charcoal and algae record from the Niayes area, Senegal, *Rev. Palaeobot. Palynol.*, 271, 104103, <https://doi.org/10.1016/j.revpalbo.2019.104103>, 2019.
- Lézine, A.-M., Izumi, K., and Achoundong, G.: Mbi Crater (Cameroon) illustrates the relations between mountain and lowland forests over the past 15,000 years in western equatorial Africa, *Quatern. Int.*, <https://doi.org/10.1016/j.quaint.2020.12.014>, in press, 2020.
- Lézine, A. M., Lemonnier, K., Waller, M. P., Bouimetarhan, I., Dupont, L., and APD contributors: Changes in the West African Landscape at the end of the African Humid Period, *Palaeoecol. Africa*, 35, 65–83, <https://doi.org/10.1201/9781003162766-6>, 2021.
- Lézine, A.-M., Catrain, M., Villamayor, J., and Khodri, M.: Using data and model to infer climate and environmental changes during the Little Ice Age in tropical West Africa, Zenodo [data set], <https://doi.org/10.5281/zenodo.7003853>, 2022.
- Lurton, T., Balkanski, Y., Bastrikov, V., Bekki, S., Bopp, L., Braconnot, P., Braconnot, P., Brockmann, P., Cadule, P., Contoux, C., Cozic, A., Cugnet, D., Ethé, C., Foujols, M. A., Ghattas, J., Hauglustaine, D., Hu, R. M., Kageyama, M., Khodri, M., Lebas, N., Levavasseur, N., Marchand, M., Otlé, C., Paylin, P., Sima, A., Szopa, S., Thiéblemont, R., Vuichard, N., and Boucher, O.: Implementation of the CMIP6 Forcing Data in the IPSL-CM6A-LR Model, *J. Adv. Model. Earth Syst.*, 12, e2019MS001940, <https://doi.org/10.1029/2019MS001940>, 2020.
- Maley, J. and Vernet, R.: Peuples et évolution climatique en Afrique nord-tropicale, de la fin du Néolithique à l’aube de l’époque moderne, *Afriques, Débats, Méthodes et Terrains d’Histoire*, OpenEdition, ISSN 2108-6796, <https://doi.org/10.4000/afriques.1209>, 2013.
- Matthes, K., Funke, B., Andersson, M. E., Barnard, L., Beer, J., Charbonneau, P., Clilverd, M. A., Dudok de Wit, T., Haber-reiter, M., Hendry, A., Jackman, C. H., Kretzschmar, M., Kruschke, T., Kunze, M., Langematz, U., Marsh, D. R., Maycock, A. C., Misios, S., Rodger, C. J., Scaife, A. A., Seppälä, A., Shangguan, M., Sinnhuber, M., Tourpali, K., Usoskin, I., van de Kamp, M., Verronen, P. T., and Versick, S.: Solar forcing for CMIP6 (v3.2), *Geosci. Model Dev.*, 10, 2247–2302, <https://doi.org/10.5194/gmd-10-2247-2017>, 2017.
- McPhaden, M. J., Zebiak, S. E., and Glanz, M. H.: ENSO as an integrating concept in earth science, *Science*, 314, 1740–1745, <https://doi.org/10.1126/science.1132588>, 2006.
- Meinshausen, M., Vogel, E., Nauels, A., Lorbacher, K., Meinshausen, N., Etheridge, D. M., Fraser, P. J., Montzka, S. A., Rayner, P. J., Trudinger, C. M., Krummel, P. B., Beyerle, U., Canadell, J. G., Daniel, J. S., Enting, I. G., Law, R. M., Lunder, C. R., O’Doherty, S., Prinn, R. G., Reimann, S., Rubino, M., Velders, G. J. M., Vollmer, M. K., Wang, R. H. J., and Weiss, R.: Historical greenhouse gas concentrations for climate modelling (CMIP6), *Geosci. Model Dev.*, 10, 2057–2116, <https://doi.org/10.5194/gmd-10-2057-2017>, 2017.
- Mohino, E., Janicot, S., and Bader, J.: Sahel rainfall and decadal to multi-decadal sea surface temperature variability, *Clim. Dynam.*, 37, 419–440, <https://doi.org/10.1007/s00382-010-0867-2>, 2011.
- Mulitza, S., Heslop, D., Pittauerova, D., Fischer, H. W., Meyer, I., Stuut, J. B., Zabel, M., Mollenhauer, G., Collins, J. A., Kuhnert, H., and Schulz, M.: Increase in African dust flux at the onset of commercial agriculture in the Sahel region, *Nature*, 466, 226–228, <https://doi.org/10.1038/nature09213>, 2010.
- Nash, D.J., De Cort, G., Chase, B. M., Verschuren, D., Nicholson, S. E., Shanahan, T. M., Asrat, A., Lézine, A. M., and Grab, S. W.: African hydroclimatic variability during the last 2000 years, *Quaternary. Sci. Rev.*, 154, 1–22, <https://doi.org/10.1016/j.quascirev.2016.10.012>, 2016.
- Ngomanda, A., Jolly, D., Bentaleb, I., Chepstow-Lusty, A., M’voubou Makaya, Maley, J., Fontune, M., Oslisly, R., and Rabenkogo, N.: Lowland forest response to hydrological changes during the last 1500 years in Gabon, Western Equatorial Africa, *Quatern. Res.*, 60, 411–425, <https://doi.org/10.1016/j.yqres.2008.12.002>, 2007.
- Nguetsop, V. F., Servant-Vildary, S., Servant, M., and Roux, M.: Long and short-time scale climatic variability in the last 5500 years in Africa according to modern and fossil diatoms from Lake Ossa (Western Cameroon), *Global Planet. Change*, 72, 356–367, <https://doi.org/10.1016/j.gloplacha.2010.01.011>, 2010.
- Nguetsop, V. F., Bentaleb, I., Favier, C., Martin, C., Bietrix, S., Giresse, P., Servant-Vildary, M., and Servant, M.: Past environmental and climatic changes during the last 7200 cal yr BP in Adamawa plateau (Northern-Cameroun) based on fossil diatoms and sedimentary carbon isotopic records from Lake Mbalang, *Clim. Past*, 7, 1371–1393, <https://doi.org/10.5194/cp-7-1371-2011>, 2011.
- Nguetsop, V. F., Bentaleb, I., Favier, C., Bietrix, S., Martin, C., Servant-Vildary, S., and Servant, M.: A late Holocene palaeoenvironmental record from Lake Tizong, northern Cameroon using diatom and carbon stable isotope analyses, *Quaternary. Sci. Rev.*, 72, 49–62, <https://doi.org/10.1016/j.quascirev.2013.04.005>, 2013.
- Nicholson, S. E.: Climatic variations in the Sahel and other African regions during the past five centuries, *J. Arid Environ.*, 1, 3–24, [https://doi.org/10.1016/S0140-1963\(18\)31750-6](https://doi.org/10.1016/S0140-1963(18)31750-6), 1978.
- Nicholson, S. E.: The nature of rainfall fluctuations in subtropical West Africa, *Mon. Weather*

- Rev., 108, 473–487, [https://doi.org/10.1175/1520-0493\(1980\)108<0473:TNORFI>2.0.CO;2](https://doi.org/10.1175/1520-0493(1980)108<0473:TNORFI>2.0.CO;2), 1980.
- Nicholson, S. E.: The West African Sahel: A review of recent studies on the rainfall regime and its interannual variability, *Intern. Scholar. Res. Not.*, Hindawi Publishing Corporation, ISRN Meteorology, 453521 <https://doi.org/10.1155/2013/453521>, 2013.
- Nicholson, S. E., Klotter, D., and Dezfuli, A. K.: Spatial reconstruction of semi-quantitative precipitation fields over Africa during the nineteenth century from documentary evidence and gauge data, *Quatern. Res.*, 78, 13–23, <https://doi.org/10.1016/j.yqres.2012.03.012>, 2012.
- Pham-Duc, B., Sylvestre, F., Papa, F., Frappart, F., Bouchez, C., and Crétaux, J. F.: The Lake Chad hydrology under current climate change, *Nat. Sci. Rep.*, 10, 5498, <https://doi.org/10.1038/s41598-020-62417-w>, 2020.
- Reynaud-Farrera, I., Maley, J., and Wirmann, D.: Végétation et climat dans les forêts du Sud-Ouest Cameroun depuis 4770 ans BP: analyse pollinique des sédiments du Lac Ossa, *C. R. Acad. Sci. Paris*, 322, 749–755, 1996.
- Rodríguez-Fonseca, B., Mohino, E., Mechoso, C. R., Caminade, C., Biasutti, M., Gaetani, M., Garcia-Serrano J., Vizy, E. K., Cook, K., Xue, Y. K., Polo, I., Losada, T., Druyan, L., Fontaine, B., Bader, J., Doblas-Reyes, F. J., Goddard, L., Janicot, S., Arribas, A., Lau, W., Colman, A., Vellinga, M., Rowell, D. P., Kucharski, F., and Voldoire, A.: Variability and predictability of West African droughts: a review on the role of sea surface temperature anomalies, *J. Climate*, 28, 4034–4060, <https://doi.org/10.1175/JCLI-D-14-00130.1>, 2015.
- Rousset, C., Vancoppenolle, M., Madec, G., Fichefet, T., Flavoni, S., Barthélemy, A., Benshila, R., Chanut, J., Lévy, C., Masson, S., and Vivier, F.: The louvain-la-neuve sea ice model LIM3.6: global and regional capabilities, *Geosci. Model. Dev.*, 8, 2991–3005, <https://doi.org/10.5194/gmd-8-2991-2015>, 2015.
- Salzmann, U. and Hoelzmann, P.: The Dahomey Gap: an abrupt climatically induced rain forest fragmentation in West Africa during the late Holocene, *Holocene*, 15, 190–199, <https://doi.org/10.1191/0959683605hl799rp>, 2005.
- Schefuß, E., Schouten, S., and Schneider, R. R.: Climatic controls on central African hydrology during the past 20,000 years, *Nature*, 437, 1003–1006, <https://doi.org/10.1038/nature03945>, 2005.
- Shanahan, T. M., Overpeck, J. T., Anchukaitis, K. J., Beck, J. W., Cole, J. E., Dettman, D. L., Peck, J. A., Scholz, A., and King, J. W.: Atlantic forcing of persistent drought in West Africa, *Science*, 324, 377–380, <https://doi.org/10.1126/science.1166352>, 2009.
- Street-Perrott, F. A., Holmes, J. A., Waller, M. P., Allen, M. J., Barber, N. G. H., Fothergill, P. A., Harkness, D. D., Ivanovich, M., Kroon, D., and Perrott, R. A.: Drought and dust deposition in the West African Sahel: a 5500-year record from Kajemaram Oasis, northeastern Nigeria, Holocene, 10, 293–302, <https://doi.org/10.1191/095968300678141274>, 2000.
- Toohey, M. and Sigl, M.: Volcanic stratospheric sulfur injections and aerosol optical depth from 500 BCE to 1900 CE, *Earth Syst. Sci. Data*, 9, 809–831, <https://doi.org/10.5194/essd-9-809-2017>, 2017.
- Tovar, C., Harris, D. J., Breman, E., Brncic, T., and Willis, K. J.: Tropical monodominant forest resilience to climate change in Central Africa: A *Gilbertiodendron dewevrei* forest pollen record over the past 2,700 years, *J. Veg. Sci.*, 30, 575–586, <https://doi.org/10.1111/jvs.12746>, 2019.
- Villamayor, J., Mohino, E., Khodri, M., Mignot, J., and Janicot, S.: Atlantic control of the late nineteenth-century Sahel humid period, *J. Climate*, 31, 8225–8240, <https://doi.org/10.1175/JCLI-D-18-0148.1>, 2018.
- Vincens, A., Schwartz, D., Bertaux, J., Elenga, H., and de Namur, C.: Late Holocene climatic changes in western equatorial Africa inferred from pollen from Lake Sinnda, southern Congo, *Quatern. Res.*, 50, 34–45, <https://doi.org/10.1006/qres.1998.1979>, 1998.
- Vincens, A., Schwartz, D., Elenga, H., Reynaud-Farrera, I., Alexandre, A., Bertaux, J., Mariotti, A., Martin, L., Meunier, J. D., Nguetsop, F., Servant, M., Servant-Vildary, S., and Wirmann, D.: Forest response to climate changes in Atlantic Equatorial Africa during the last 4000 years BP and inheritance on the modern landscapes, *J. Biogeogr.*, 26, 879–885, <https://doi.org/10.1046/j.1365-2699.1999.00333.x>, 1999.
- Vincens, A., Buchet, G., and Servant, M.: Vegetation response to the “African Humid Period” termination in Central Cameroon (7° N) – new pollen insight from Lake Mbalang, *Clim. Past*, 6, 281–294, <https://doi.org/10.5194/cp-6-281-2010>, 2010.
- Waller, M. P., Street-Perrott, F. A., and Wang, H.: Holocene vegetation history of the Sahel: pollen, sedimentological and geochemical data from Jikariya Lake, north-eastern Nigeria, *J. Biogeogr.*, 34, 1575–1590, <https://doi.org/10.1111/j.1365-2699.2007.01721.x>, 2007.
- Wang, H., Holmes, J. A., Street-Perrott, F. A., Waller, M. P., and Perrott, R. A.: Holocene environmental change in the West African Sahel: sedimentological and mineral-magnetic analyses of lake sediments from Jikariya Lake, northeastern Nigeria, *J. Quaternary Sci.*, 23, 449–460, <https://doi.org/10.1002/jqs.1154>, 2008.
- White, F.: The vegetation of Africa, UNESCO, Paris, ISBN 9231019554, 1983.